Arch. Metall. Mater. **63** (2018), 3, 1303-1315

DOI: 10.24425/123805

N. JEYAPRAKASH*, M. DURAISELVAM*#, R. RAJU**

MODELLING OF Cr_3C_2-25% NiCr LASER ALLOYED CAST IRON IN HIGH TEMPERATURE SLIDING WEAR CONDITION USING RESPONSE SURFACE METHODOLOGY

The wear behaviour of Cr_3C_2-25% NiCr laser alloyed nodular cast iron sample were analyzed using a pin-on-disc tribometer. The influence of sliding velocity, temperature and load on laser alloyed sample was focused and the microscopic images were used for metallurgical examination of the worn-out sites. Box-Behnken method was utilised to generate the mathematical model for the condition parameters. The Response Surface Methodology (RSM) based models are varied to analyse the process parameters interaction effects. Analysis of variance was used to analyse the developed model and the results showed that the laser alloyed sample leads to a minimum wear rate (0.6079×10^{-3} to 1.8570×10^{-3} mm^3/m) and coefficient of friction (CoF) (0.43 to 0.53). From the test results, it was observed that the experimental results correlated well with the predicted results of the developed mathematical model.

Keywords: Laser Surface Alloying (LSA); Wear; Microhardness; Analysis of Variance (ANOVA); Response Surface Methodology (RSM)

1. Introduction

The automotive sector is increasing the usage of novelty steels like Nodular Cast Iron (NCI) in cams, pipes, engine blocks, beds and various machine parts manufacturing due to their excellent machinability, good fluidity, low melting point and castability. [1,2]. However, a series of new technical problems has arisen under severe working conditions due to wear. It affects the performance and reliability of the structural components and decreases the service life. Therefore, the application of a novel surface modification technology is necessary to improve the service life of NCI parts with higher performance.

Laser surface engineering, which is based on the principle of laser material surface modification and/or manufacturing, has been recognized as a promising technology than rest of surface modification methods, due to its flexibility and a non-equilibrium method to produce higher cooling rates (10^3-10^8 Ks^{-1}) [3,4]. Several microstructural variations with unique properties that cannot be produced using conventional technique can be attained through laser processing [5]. Laser processing includes quenching [6], surface hardening [7], surface melting [8-10], laser surface alloying (LSA) [11,12] and cladding [13,14]. The principle behind the LSA process contains the formation of metallurgically bonded coating by melting alloy powders such as tungsten, nickel, chromium and tungsten-cobalt-vanadium-chromium onto the substrate surface with a laser beam normal to the substrate [15].

The alloying of tough Cr_3C_2-25% NiCr with the substrate through surface alloying process enhances the wear properties. The commonly used Cr_3C_2-25% NiCr have good chemical, mechanical and higher wear resistant property. The wear properties can be increased on the Cr_3C_2-25% NiCr coatings, by reducing the particle grain size. The smaller size of the Cr_3C_2 particles supports in holding the disarray thus greatly improving the wear resistance [16]. Due to the superior hardness and wear resistant property, Cr_3C_2-25% NiCr alloy powder is widely used as wear resistant coating in mechanical industries.

A number of experimental techniques have been proposed to mitigate the effect of tribological properties on LSM substrates. However, experimental trials consume more time, high cost and manpower. To overcome this, many researchers were applied modelling techniques to obtain optimal condition of the parameter through model expansion without spending more time. Hence, a suitable mathematical formulation such as Design of Experiment (DOE) was adopted. DOE is a technique to develop mathematical model using scientific methods like ANOVA which shows the connection among responses and input criteria [17]. RSM and DOE methods are used for creating the experimental design, identifying the scientific model, finding the optimal parameters that produces the determined responses and signifying the collective effects of process variables over 3D and 2D graphs [18].

Kumar et al. [19] performed wear test to study the wear mechanism of aluminum alloys by differing load, distance and

* NATIONAL INSTITUTE OF TECHNOLOGY, DEPARTMENT OF PRODUCTION ENGINEERING, TIRUCHIRAPPALLI 620015, TAMIL NADU, INDIA
** SANTHIRAM ENGINEERING COLLEGE, DEPARTMENT OF MECHANICAL ENGINEERING, NANDYAL 518502, ANDHRA PRADESH, INDIA
# Corresponding author: durai@nitt.edu

sliding speed. The major factor that influenced the wear rate was determined using RSM technique. It was reported that applied load had maximum effect among all other parameters. The sliding distance and speed had the secondary influence. Lin et al. [20] investigated the wear mechanism by using central composite design (CCD) method through RSM technique. A second order polynomial represented a curved surface that fitted the trial data and obtained wear rate, CoF and temperature as the speed and load function. Farias et al. [21] studied the tribological properties of austenitic steel and developed a scientific model for load and velocity based on wear rate through RSM method. The interaction between tangential load and velocity provide the rate of wear. Sahin et al. [22] studied the abrasive wear mechanism of aluminum based composites through tribo testing and determined distance, load and size of particle using factorial design. The increase in abrasive size and applied load enhanced the wear rate while it decreased with greater sliding distance**.**

From the literature survey, it was inferred that the tribological properties of several metals were experimentally investigated. The effect of applied load, sliding velocity and sliding distance were assessed by the experimental work. The major significance of this present research work is to emphasis the effects of input criteria like sliding velocity, temperature and load on the dry condition. The wear mechanism was analysed in the laser alloyed surfaces. The process input criteria was used to calculate the tribo test responses. The process input criteria had a nonlinear affinity with the responses interconnected as well. Hence, the selection of input criteria was essential for investigating the responses like CoF and wear rate. By using RSM and DOE, the interactive and direct effects of process criteria with responses were studied.

2. Experimental procedure

2.1. Experimental material

The experimental material for laser alloying is Cr_3C_2-25% NiCr alloy powder of near spherical shape having particle size about 20-80 μm. The SEM observation of Cr_3C_2-25% NiCr powder is shown in Fig. 1. The NCI blocks with nominal size of 25×25×30 mm were used as the substrate material. The chemical composition of the substrate material is given in Table 1. The blocks were cleaned with 320 grade silicon carbide grit paper and the surface was refined using alumina paste to obtain a surface roughness of 10 μm. The laser alloyed specimen was cut in to pin shape for wear test having dimension of 6×6×30 mm.

2.2. Laser surface alloying

The commercially available Cr_3C_2-25%NiCr powder (Oerlikon metco) was used in this study and a 3 kW fiber laser beam was raster scanned over the substrate to melt and fuse the alloy with the substrate. The process parameters were used in this experiment is listed in Table 2. The samples are irradiated under argon atmosphere (3 bar) to avoid the atmospheric contamination. After preplacing the powder, laser surface alloying was performed. The elemental distribution was identified by EDS. During laser scanning, the alloy powder got melted and alloyed along with the base material for 950 μm depth during laser scanning. The PVA binder was evaporated during laser exposure. The samples were exposed to a continuous wave laser

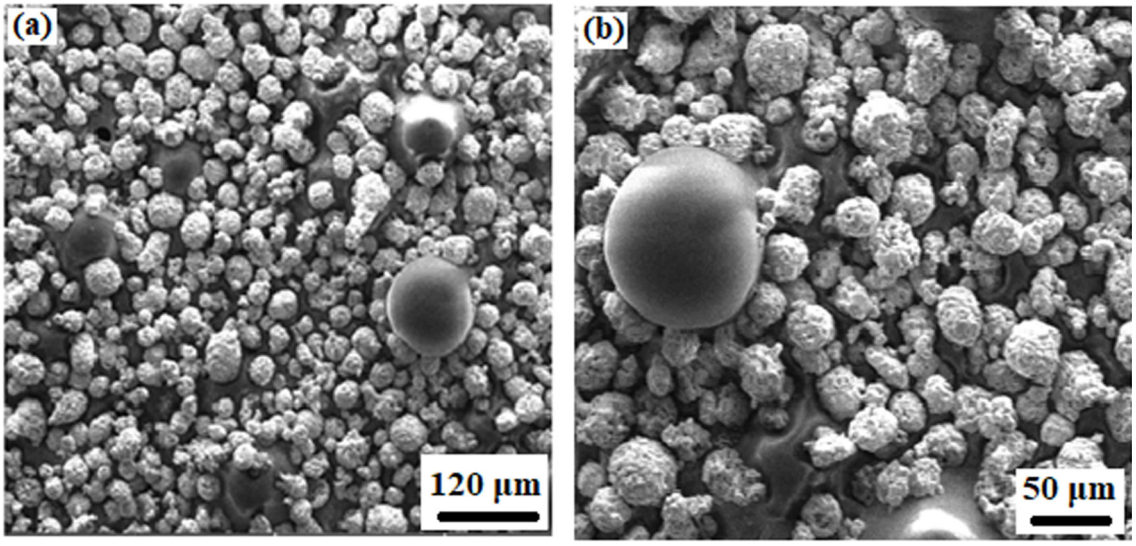

Fig. 1. SEM images of (a) as received Cr_3C_2-25% NiCr alloy powder (b) magnified view

TABLE 1

Chemical Composition of Nodular Cast Iron (SG 450-10)

Element	Fe	C	Si	Mn	P	S	Mg	Cr	Cu
Wt (%)	Bal.	3.69	3.16	0.610	0.0620	0.0220	0.0280	0.0350	0.218

surface alloying under three different conditions. The Cr_3C_2-25% NiCr coating cross section is shown in Fig. 2.

TABLE 2

Process parameters used for LSA

Parameter	Value
Laser Power (kW)	1-1.5
Laser scan speed (mm/min)	300-600
Defocus distance (mm)	15-20
Overlapping (%)	30

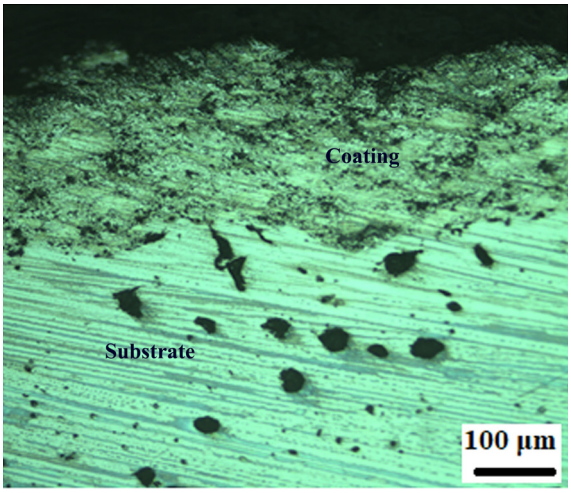

Fig. 2. Cross-section of preplaced coating of Cr_3C_2-25% NiCr

The optimum laser process parameter values were selected depending on the defect free and sufficient alloyed depth of the sample. The surfaces alloyed at 1 kW and 300 mm/min scan speed with defocus of 20 mm resulted in surface crack and alloyed at 1.5 kW and 600 mm/min scan speed with 20 mm defocus resulted in insufficient depth. The 1.5 kW and 600 mm/min scan speed with 15 mm defocus exhibited with optimal laser parameter in the present experiment.

2.3. Wear test

Dry sliding wear test on LSA specimen were performed using a pin-on-disc tribometer (TR-20LE-PHM 400-CHM 500) at high temperature as per ASTM G99-05 standard [23]. A 100 mm diameter and 5 mm thick hardened steel disc was taken as the counter face material. Load, sliding velocity and temperature with constant sliding distance (1000 m) was selected as the wear testing parameters. The mass loss of the pin was calculated before and after each wear test. An electronic weighing balance having 0.1 mg accuracy was employed to measure mass loss. The volume loss (V), sliding distance (L), wear rate (ω) and CoF (μ) were calculated using Equations 1-4.

$$V = \frac{M_{loss}}{\rho} X 1000 \quad (1)$$

Where M_{loss} is weight loss of the specimen and ρ is the density.

$$L = \pi ZRP \quad (2)$$

Where Z is the mean diameter of the wear track (m), R is the rotational speed (rpm), and P is the time (min).

$$\omega = \frac{V}{L} \quad (3)$$

$$\mu = \frac{F}{N} \quad (4)$$

Where N is the normal load and F is the frictional force.

2.4. Characterization

The laser alloyed specimen was cross-sectioned by wire EDM for microhardness and microstructural studies. The specimen was polished using standard metallographic techniques and then etched with Murukamis etching reagent ($K_3Fe(CN)_6$, NaOH and Distilled water) in the ratio of 10:1:1. Scanning Electron Microscopy (SEM) (TESCAN) was used to examine the microstructure, surface morphology of laser alloyed specimens before and after wear test. The EDAX analysis was done to understand the alloy powder distribution in to the substrate. The microhardness was measured using Wolpert Wilson Vickers microhardness tester using test load of 300 g for a dwell time of 10 s.

3. Mathematical modelling by RSM

The optimization through RSM has been applied to develop, improve and optimize numerous processes [24,25]. Many input variables strongly influence the quantified weight of each parameter and performance measure. RSM involves the experimental approach for analysing the area of the absolute variables and empirical statistical modelling for creating a suitable close relationship among the input variables and responses.

3.1. Experimental design

The influence of process parameters i.e. sliding velocity, working temperature and applied load has been investigated against the wear rate and CoF of laser alloyed NCI. Design expert software was employed to statistically analyse and develop mathematical models. The process windows were created as explained elsewhere [26]. The three factors of three levels Box-Behnken design was used to analyse the main effects of laser surface treated specimens. The response functions, wear rate and CoF is a function of applied load (A), sliding velocity (B) and working temperature (C) and they can be expressed as

$$\text{CoF} = f(\text{A,B,C}) \quad (5)$$

$$\text{Wear rate} = f(\text{A,B,C}) \quad (6)$$

The second order polynomial regression equation used to signify the response surface Y for the chosen input parameters is given in Equation 7.

$$Y = b_0 + \sum_{i=1}^{k} b_i x_i + \sum_{i=1}^{k} b_{ii} x_i^2 + \sum_{i=1}^{k-1} \sum_{j=2}^{k} b_{ij} x_{i\,X\,j} \quad (7)$$

Where b_{ij} = 0,1, ...k and b_0 is the arithmetic average of all outcomes

Table 3 and 4 represents respectively the ranges of factors considered and the set of conditions used to form the design matrix.

TABLE 3

Independent process variables and experimental design levels

S. No	Factor	Notations	Unit	Levels		
				–1	0	+1
1	Applied load	A	N	10	20	30
2	Sliding velocity	B	m/s	0.5	1	1.5
3	Temperature	C	˚C	40	170	300

TABLE 4

Design matrix and experimental results of laser alloyed samples

Variables					Laser alloyed Responses	
Std. Order	Run Order	Applied load	Sliding Velocity	Tempe-rature	Wear rate × 10^{-3} (mm^3/m)	CoF
1	12	20	1.5	300	1.3860	0.45
2	13	20	1.0	170	1.0346	0.46
3	3	10	1.5	170	0.8431	0.48
4	16	20	1.0	170	1.0621	0.47
5	1	10	0.5	170	0.6079	0.53
6	6	30	1.0	40	1.6380	0.48
7	9	20	0.5	40	0.8810	0.46
8	15	20	1.0	170	1.0247	0.45
9	14	20	1.0	170	1.0421	0.44
10	17	20	1.0	170	0.9984	0.43
11	2	30	0.5	170	1.5530	0.45
12	7	10	1.0	300	0.7570	0.52
13	5	10	1.0	40	0.7230	0.52
14	8	30	1.0	300	1.8570	0.49
15	11	20	0.5	300	0.9450	0.48
16	4	30	1.5	170	1.8349	0.46
17	10	20	1.5	40	1.1831	0.47

3.2. Modelling

The experimental results are analysed using RSM to find the accurate model for best response. The centre point or local region of the model is determined to have efficient relation with the predicted response [27]. The mathematical connection between the responses and input criteria are clarified by the quadratic model [28]. The regression model was developed for the CoF and wear rate of laser alloyed sample (Equations 8 and 9).

$$\text{CoF} = 0.45\text{-}0.021\text{A}\text{-}7.500\text{E-}003\text{B}+1.250\text{E-}003\text{C}+ +0.015\text{AB}+2.500\text{E-}003\text{AC}\text{-}1.000\text{E-}002\text{BC}+ +0.034\ \text{A}^2\text{-}3.750\text{E-}003\text{B}^2+0.019\text{C}^2 \quad (8)$$

$$\text{Wear rate} = 1.03+0.49\text{A}+0.16\text{B}+0.065\text{C}+ +0.012\text{AB}+0.046\text{AC}+0.035\text{BC}+0.16\text{A}^2+ +0.016\text{B}^2+0.050\text{C}^2 \quad (9)$$

3.3. Testing the data and adequacy of model

3.3.1. Normality of the data

Normal probability plot performs normality of the input [29]. Fig. 3 gives the normal probability plots of the residuals for the wear rate and CoF for laser alloyed samples. From the wear rate and CoF plot, it was evident that the residuals were falling on the straight line. Hence, the errors were found to be distributed normally.

3.3.2. Independency of the data

A graph between residuals and run order was plotted to verify the input independency [30]. Fig. 4 shows the residual graph for wear rate and CoF for laser alloyed samples. In all the wear rate and CoF graphs, run balance was present between –3 to +3 level which indicated that there was no predictable pattern observation [31].

3.3.3. Analysis of variance

The developed model is determined using analysis of variance (ANOVA) method. The coefficient of determination (R^2) is calculated to predict the fitness for the developed model. The model is adequate within the confidence level, if the calculated F value of the developed model is greater than the standard tabular F value [29].

The ANOVA outcome of the rate of wear for laser alloyed samples is given in Table 5. It is understood that the developed model is adequate at 99% confidence level, since the value of P is 0.0001. The reliability of equation (9) was signified by determining the wear rate for laser alloyed sample (R^2) which was 0.99598. In addition, the model F-value is so high than the tabular value $F_{0.01\,(9,\,7)}$ which indicates the model is more significant. The value of Adeq. Precision is 46.4425 which is apparently grater and makes the model discrimination. As the obtained R^2 value is near to 1, the developed mathematical model is in good agreement with the experimental data.

Table 6 shows the ANOVA outcomes of the CoF for laser alloyed sample which specifies that certainty of the developed model for CoF is at 91% confidence level. The reliability of Equation (8) was signified by determining the CoF for laser alloyed sample (R^2) which was 0.91066. In addition, the model F-value

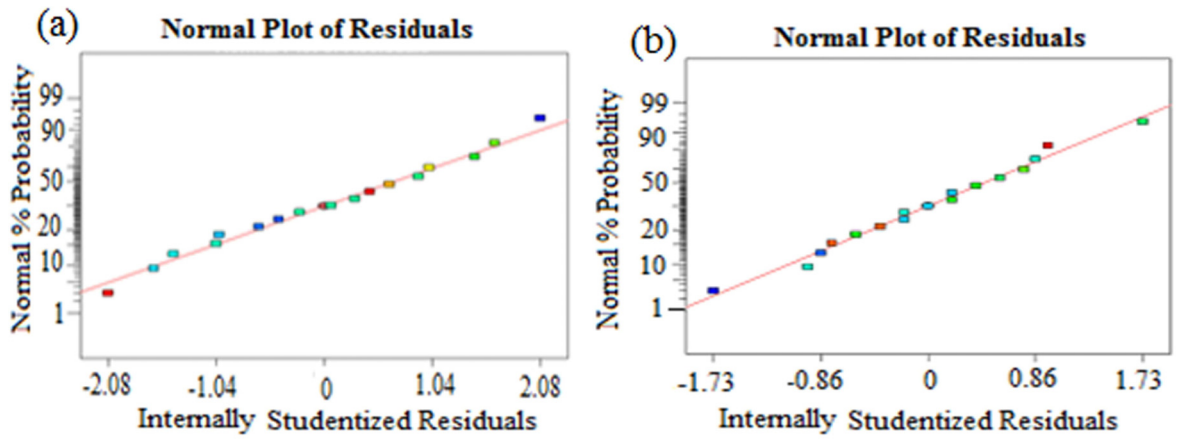

Fig. 3. Normal probability plots for laser alloyed sample (a) wear rate (b) CoF

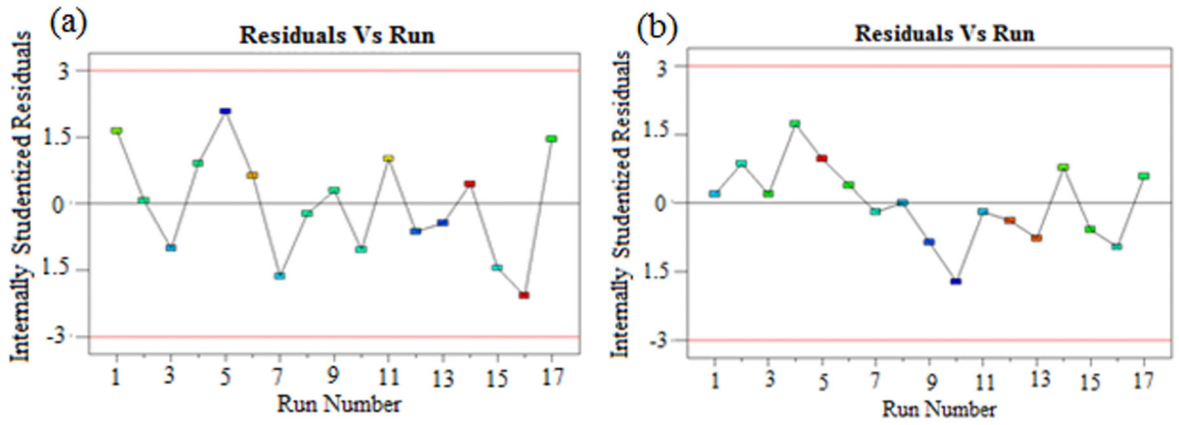

Fig. 4. Residual plots for laser alloyed sample (a) wear rate (b) CoF

TABLE 5

ANOVA results of the Wear rate for laser alloyed sample using suggested quadratic model

Source	Sum of Squares	DF	Mean Square	*F* Value	*p*-Value prob > *F*	
Model	2.32562	9	0.25840	193.09	<0.0001	signifi-cant
A	1.95218	1	1.95218	1458.81	<0.0001	
B	0.19851	1	0.19851	148.34	<0.0001	
C	0.03378	1	0.03378	25.24	0.0015	
AB	0.00054	1	0.00054	0.40742	0.5436	
AC	0.00855	1	0.00855	6.39384	0.0393	
BC	0.00482	1	0.00482	3.60431	0.0994	
A^2	0.10935	1	0.10935	81.7201	<0.0001	
B^2	0.00110	1	0.00110	0.82421	0.3941	
C^2	0.01061	1	0.01061	7.93223	0.0259	
Residual	0.00936	7	0.00133			
Corrected total	2.33498	16				
SD	0.03658		R^2	0.99598		
Mean	1.13946		Adj.R^2	0.99083		
Coefficient of Variation (%)	3.21040		Pred.R^2	0.94939		
PRESS	0.11816		Adeq. precision	46.44259		

TABLE 6

ANOVA results of the CoF for laser alloyed sample using suggested quadratic model

Source	Sum of Squares	DF	Mean Square	*F* Value	p-Value prob> F	
Model	0.01197	9	0.00133	7.92866	0.0062	signifi-cant
A	0.00361	1	0.00361	21.5212	0.0024	
B	0.00045	1	0.00045	2.68085	0.1456	
C	1.25E-05	1	0.00001	0.07446	0.7928	
AB	0.0009	1	0.0009	5.36170	0.0537	
AC	2.5E-05	1	2.5E-05	0.14893	0.7110	
BC	0.0004	1	0.0004	2.38297	0.1666	
A^2	0.00479	1	0.00479	28.5722	0.0011	
B^2	5.92E-05	1	5.92E-05	0.35274	0.5713	
C^2	0.00148	1	0.001480	8.81858	0.0208	
Residual	0.00117	7	0.000167			
Corrected total	0.01315	16				
SD	0.01295		R^2	0.91066		
Mean	0.47294		Adj.R^2	0.79580		
Coefficient of Variation (%)	2.73944		Pred.R^2	0.66832		
PRESS	0.00436		Adeq. precision	7.67351		

of 7.92 is higher than the tabular value $F_{0.01\,(9,\,7)}$ of 6.72 which indicates ANOVA response of this model is more significant.

4. Results and discussion

4.1. Microstructure examination

The SEM micrograph of the as-received NCI is shown in Fig. 5a-b. The microstructure consists of nodular graphite dispersed in a ferritic matrix. After laser alloying, microstructural study indicates the presence of Cr_3C_2-25% NiCr elements in the alloyed zone and is shown in Fig. 5c-d. The cross sectioned laser alloyed sample exhibited no defects such as micro-cracks or pits. The microstructure of the alloying regions shows that fine and homogeneous structure. Higher cooling rate dissolved the graphite nodules. The dissolution of graphite under the interaction of laser was also reported by Gulzar et al [32]. The higher cooling rate attributed the formation of fine cellular dendrite structure. The formation of ledeburite structure was reported by several investigators [32-34]. This fine dendritic structure was reported to enhance the tribological properties.

The micrograph of Cr_3C_2-25% NiCr confirms the porous nature and the presence of needle like structure indicating the granular dispersion in the matrix phase. This indicates that a great cooling rate over solidification process. The cooling rate and high thermal gradient produced robust convection thereby resulting a homogeneous structure formation. Also, it is noticeable from the micrographs that complete dissolution of graphite nodules along with alloy powder through laser alloying process and fast self-quenching the re-formation of cast iron in the formation of hard Cr_3C_2-25% NiCr alloyed surface.

4.2. Microhardness analysis

The hardness profile along the width and depth of laser alloyed zone are shown in Fig. 6a. It was observed that the laser alloyed region had average hardness of 905 $HV_{0.3}$, which was greater than substrate material hardness (220 $HV_{0.3}$). The alloy powder Cr_3C_2-25% NiCr was completely fused and inter mixed with the substrate metal uniformly as shown by the EDX analysis. It was proved experimentally that when a hard particle was fused into a softer surface, the hardness of the softer surface was

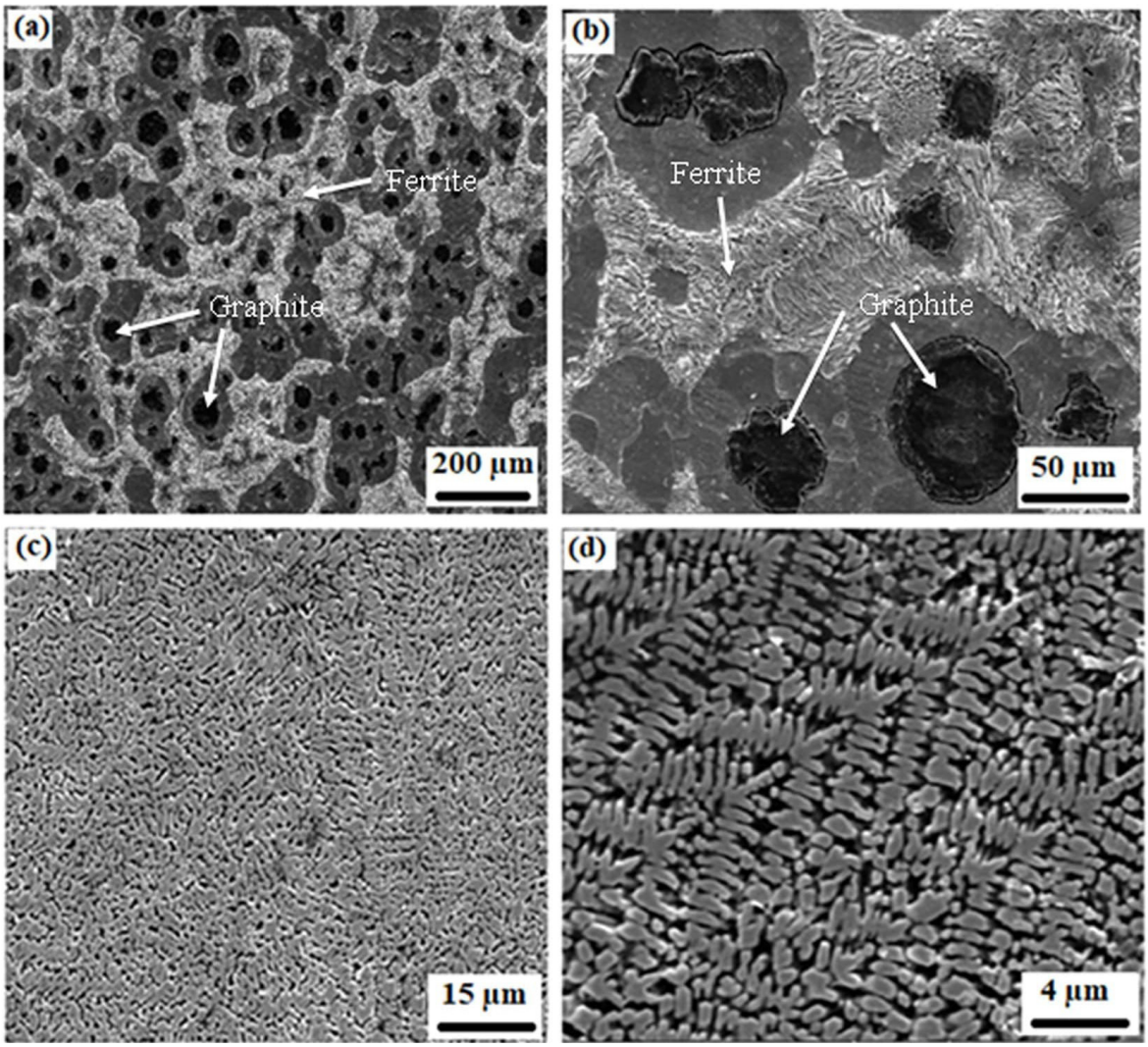

Fig. 5. SEM image of (a and b) untreated sample, (c and d) laser alloyed cross section

enhanced [35]. Also, numerous other researchers have noticed similar behaviour in fusion of hard particle into softer surface and the results were in accordance with the findings of Li Pengting et al. [36]. After laser alloying with Cr_3C_2-25% NiCr the hardness was enhanced by 4.11 times.

This was due to the fine cellular dendrite structure that confined the plastic distortion produced by the indenter. Hence, the lengthened needle like structure provided greater reinforcement to the laser alloyed region as shown in Fig. 6b.

4.3. Elemental analysis

The result of elemental analysis is shown in Fig. 7a and the mass fraction (%) as follows: Fe 40.89, Cr 20.34, Ni 5.46, C 13.13 and O 17.63. The Cr, Ni and C elements were evenly distributed over the alloyed surface [Fig. 7d-f]. This signifies the good integrity of the laser alloyed surface. The distribution of Fe and O were also distributed evenly [Fig. 7c,g]. During LSA, the diffusion of Fe atoms is attributed through the metallurgical

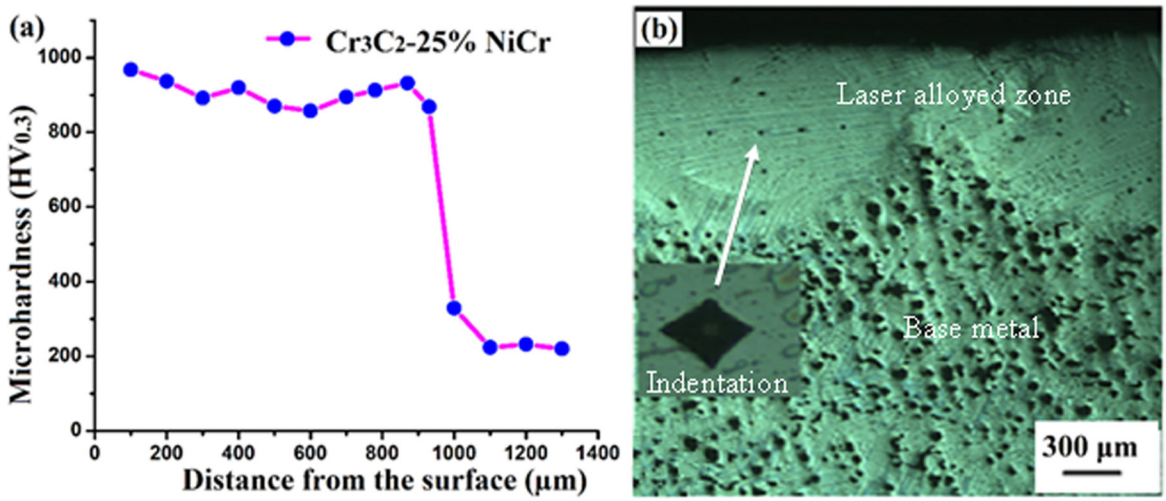

Fig. 6. (a) Microhardness of laser alloyed cross section (b) Indentation of hardness measurement

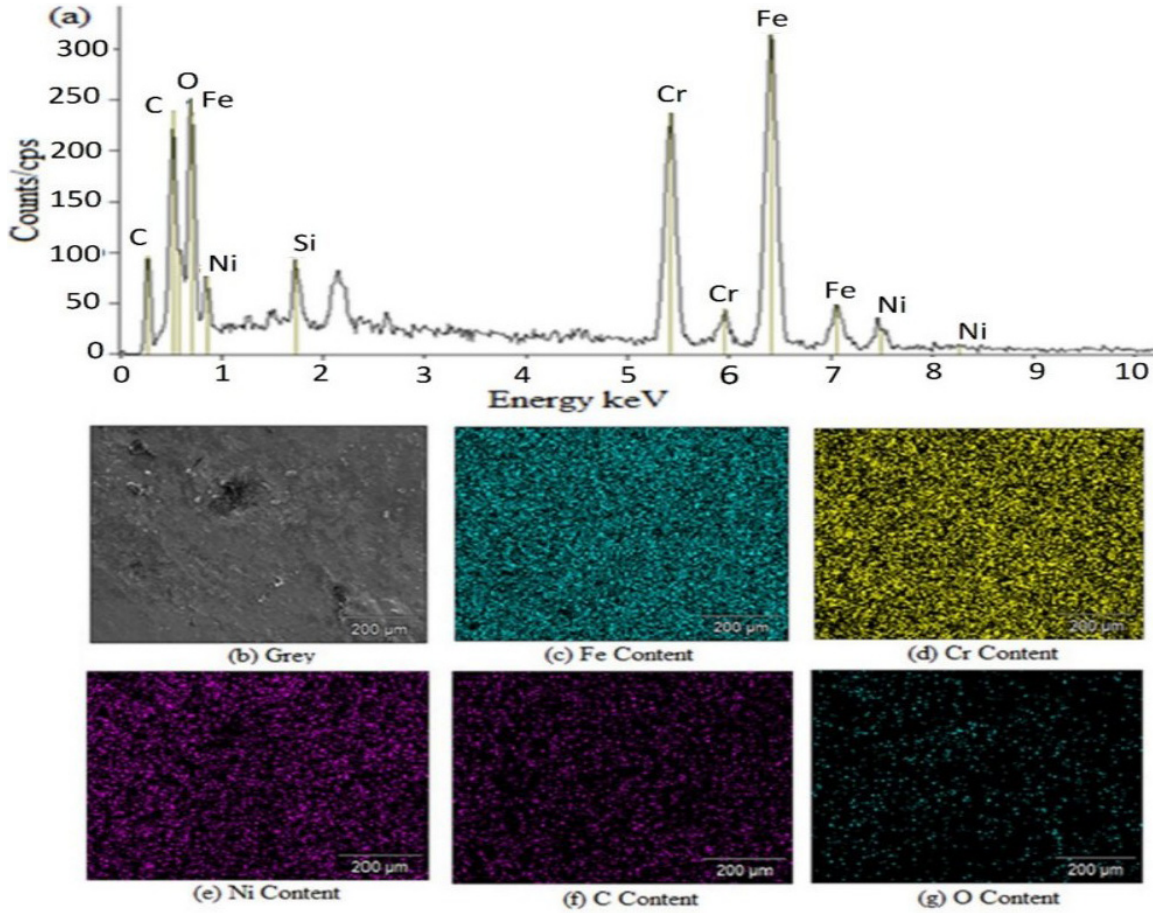

Fig. 7. EDS elemental mapping of laser alloyed surface

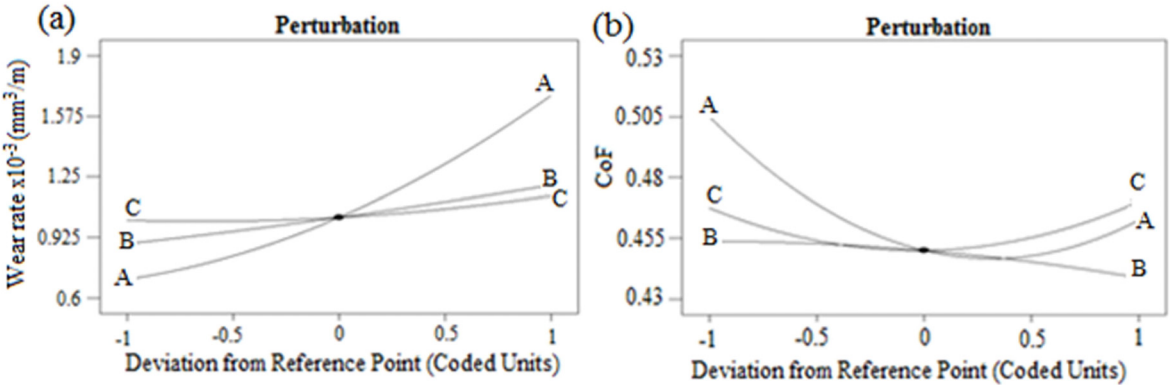

Fig. 8. Perturbation plot for laser alloyed sample (a) wear rate and (b) CoF

combination between the alloying elements and the substrate elements. The presence of O was originated through the oxidative reaction during LSA.

4.4. Perturbation plot

The perturbation plots for rate of wear shown in Fig. 8a relates the results of trial criterion on the wear rate at the centre point. The rate of wear increased with higher load. The frictional heat generated at the contact area and material strength decreases. The rate of wear increased with sliding velocity and temperature but effect is less.

The perturbation plot given in Fig. 8b relates the reaction of input parameters at midpoint on the CoF. The CoF decreases with increased load and sliding velocity. This is due to the fact that variation in the rate of shear significantly influences the mechanical properties. The materials exhibit improved strength at higher shear-strain rates [37,38]. This higher rate reduces the real contact area and minimise the CoF in dry contact condition. These findings correlate well with the work reported by Chowdhury and Helali [39]. The CoF increased with rising the temperature. However, the temperature had a lesser influence on CoF.

4.5. Laser alloyed sample

4.5.1. Interaction effect on wear rate

Fig. 9a,b represents the 3D and 2D interaction effect of applied load and sliding velocity. From 3D plot (Fig. 9a) it was observed that rate of wear increased with higher load and sliding velocity.

The results can be identified with 2D plots showing various colors mainly red for high, green for medium and blue for low value for wear rate. The wear rate was minimal when load is less than 20 N with medium velocity. The wear rate was moderate when applied load reached 20 N due to oxide layer formation. Higher load and sliding velocity increased the rate of wear because of broken oxide layer. Fig. 9c,d represents the interaction effect of temperature and load on wear rate. The 3D plot showed that wear rate increased by maximizing the load and temperature. At 15 N load with 40°C, wear rate was minimal. When temperature crossed 170°C, the wear rate gradually increased up to 300°C for load between 25 and 30 N. Fig. 9e,f shows the effect of sliding velocity and temperature on wear rate. The 3D plot (Fig. 9e) confirmed that the wear rate was fairly increased when increasing the sliding velocity and temperature. However, there was no much influence of temperature for wear rate. The presence of red region was not identified which implies that higher wear rate value was not obtained.

4.5.2. Interaction effect on CoF

Fig. 10a,b indicates the effects of applied load and sliding velocity over CoF. From Fig. 10a, it was inferred that the CoF is higher at a combination of high load and low sliding velocity. The results notified that 2D plot had three colors namely, red for maximum, green for medium and blue for minimum CoF. When increasing the applied load and sliding velocity, CoF was decreased. Fig. 10c,d depicts the effect of responses of temperature and load on CoF. It can be determined that while increasing the temperature, CoF was increased.

The increase in load from 25 N to 30 N resulted in the increase of CoF. The results indicated that 2D plot had three different colors namely, red for high, green for medium and blue for less CoF. Due to oxide layer formation, at medium load (20 N), the CoF was minimum at medium level of temperature. Fig. 10e,f shows the 3D and 2D response effect of sliding velocity and temperature on CoF. The CoF fairly increased when increasing the temperature and when increasing the sliding velocity, CoF decreased. However, temperature and sliding velocity had a little influence on CoF. Since, there was no red region, higher CoF was not obtained.

4.6. Validation

Three sets of values were chosen randomly to run the validation trials and to confirm the developed mathematical model. For evaluation, all experiments were repeated three times. The

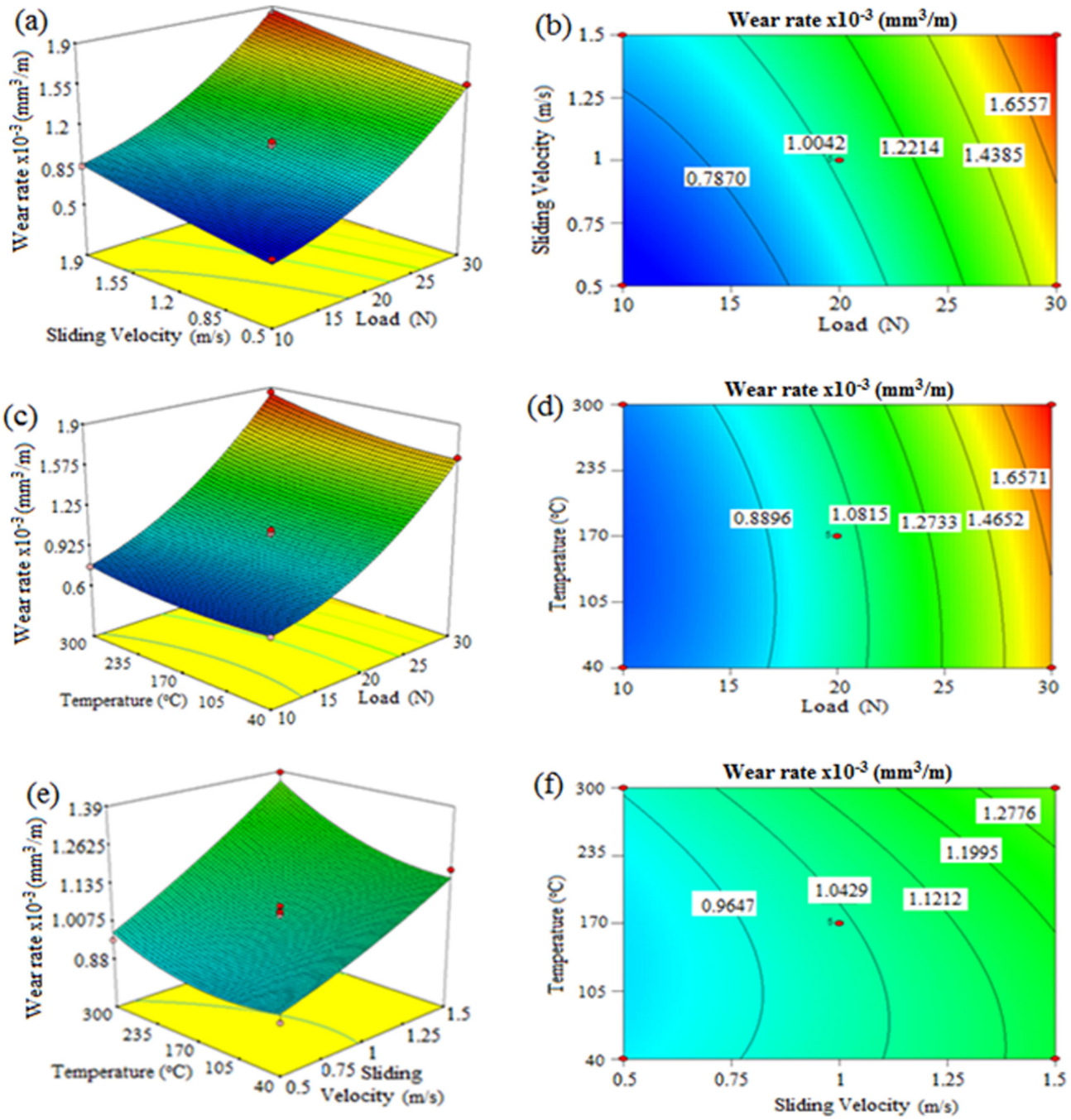

Fig. 9. Interaction plot for wear rate of laser alloyed sample: (a), (c), (e) 3D plot and (b), (d), (f) 2D plot

original value of the outcomes was measured as the average of three experiments. The connection between experimental and predicted values of the CoF and wear rate for laser alloyed samples is shown in Fig. 11. From the Figure it was evident that the developed models were unique and the predicted values were found to be in good agreement with measured data.

4.7. Worn surface topography

SEM images (Fig. 12) were taken for the worn out surfaces of laser alloyed surface. To reveal the variance in the wear, worn surface of SEM images, after trial at maximum load and sliding velocity with the sliding distance of 1000 m was explained. In laser alloyed specimen, the surface of the sample got scratched less. The laser alloyed surfaces showed lower material loss due to the deposition of the harder Cr_3C_2-25% NiCr. When the counterpart comes in contact with the pin surface, the hard extended part of the disc pressed the laser alloyed surface. As a result, adhesion and scuffing occurred [40], which hindered the movement between the disc and pin. However, wear rate and CoF was minimum. The depth of the wear track was less and pile-up of material were minimum on the plow marks. The finer groove marks were visible on laser alloyed worn surface. The finer grooves indicated lesser material loss from the laser alloyed surface. This was due to elongated eutectic carbides which

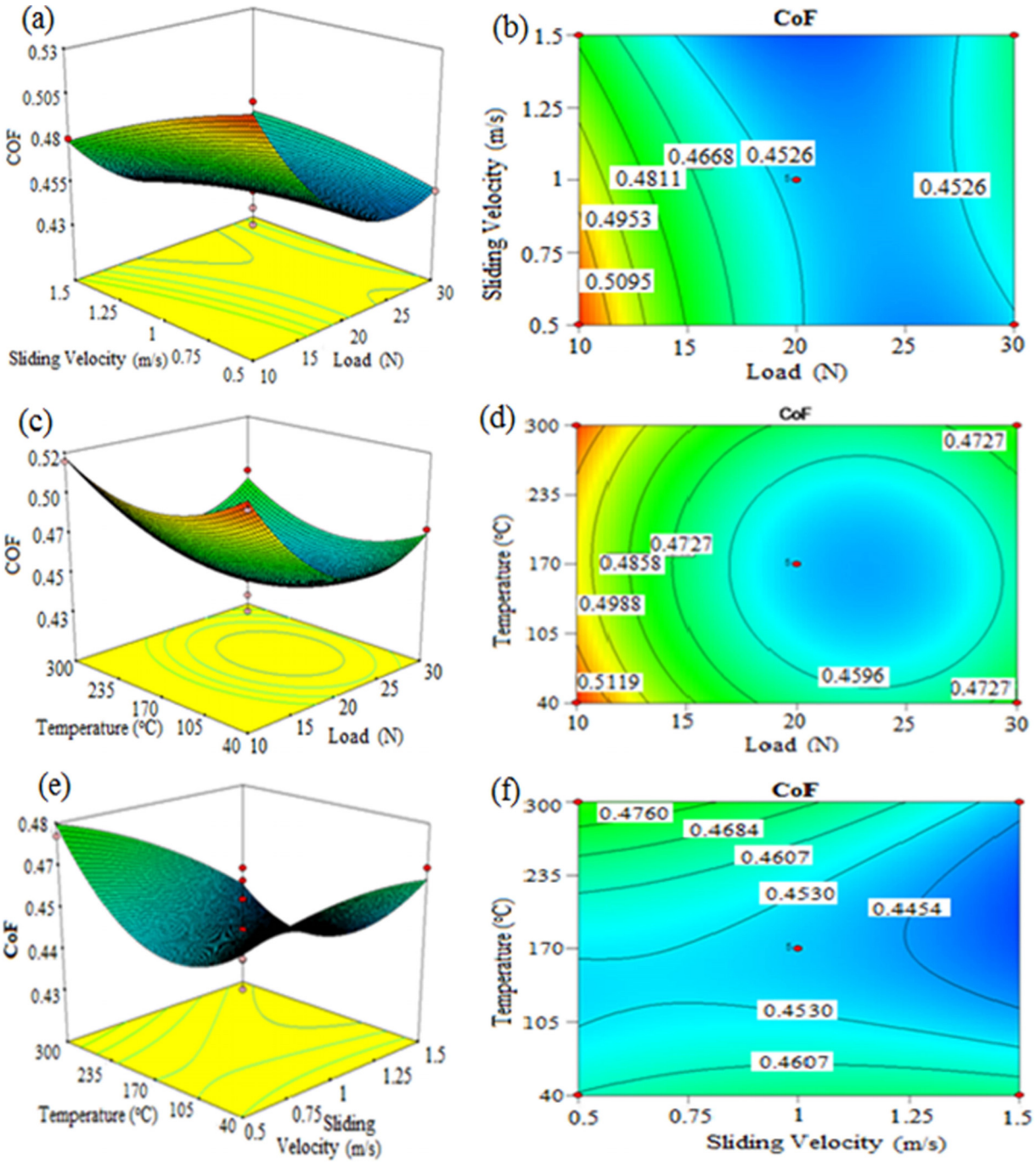

Fig. 10. Interaction plot for CoF of laser alloyed sample: (a), (c), (e) 3D plot and (b), (d), (f) 2D plot

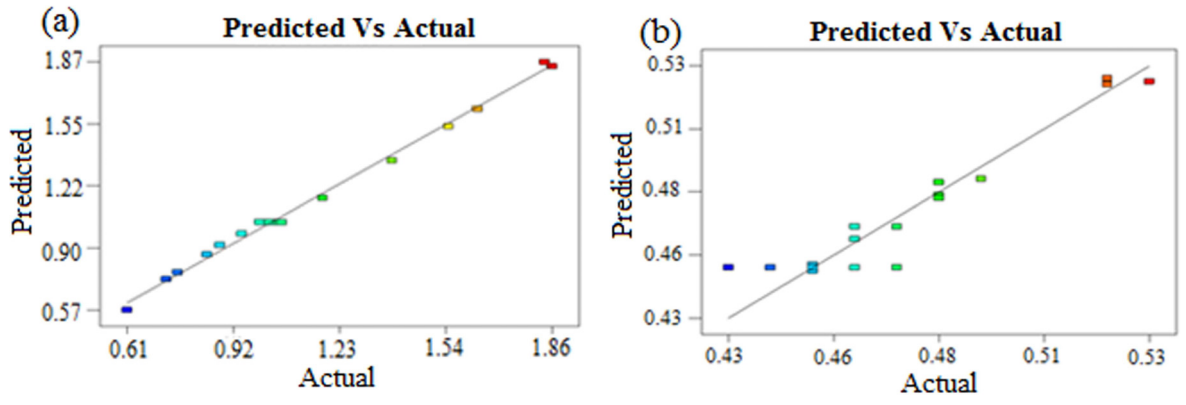

Fig. 11. Relationship between predicted and experimental values of laser alloyed sample (a) Wear rate (b) CoF

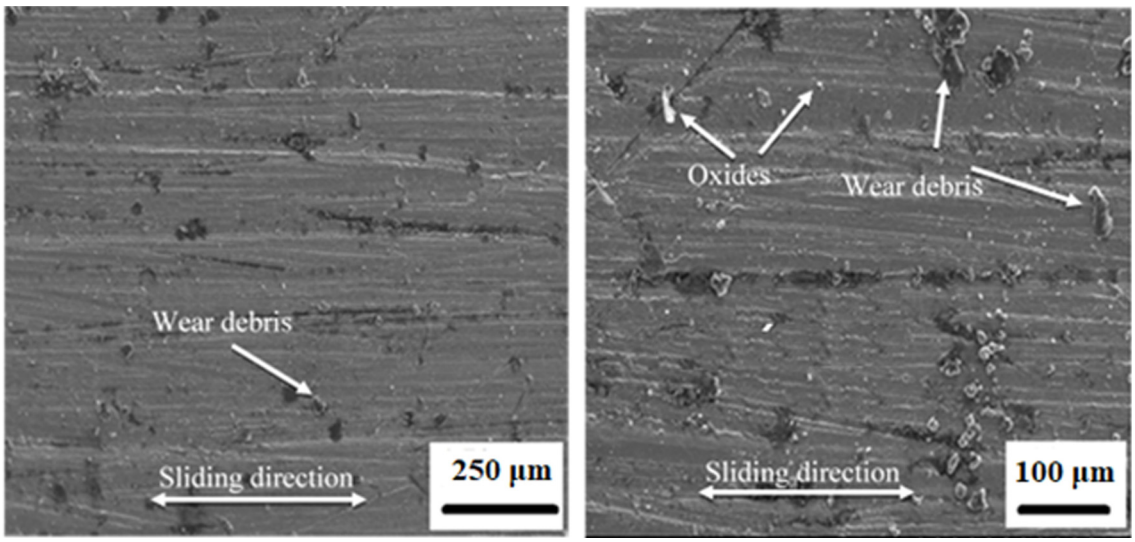

Fig. 12. SEM micrographs of worn out surfaces of laser alloyed sample

resulted in higher hardness of laser alloyed surface. The harder Cr_3C_2-25% NiCr alloyed surfaces improved the strength against abrasion and enhanced the wear resistance. It was clear that the laser alloyed surface exhibited good wear resistance to abrasion.

4.8. Wear mechanism

The metal removal system map was refined to show and discuss the wear mechanism in single plot. A 2D plot was made between load and sliding velocity to the parallel value of wear rate and SEM observation was used to categorize oxidation, abrasion, delamination and severe wear. The SEM images showed the worn out surface of laser alloyed sample after high temperature wear test under the applied sliding velocity and load.

At 10 to 15 N load with medium velocity, finer scratches were noticed parallel to the sliding direction and exhibited an abrasive wear mechanism. The harder asperities present over the steel counterpart ploughed the pin material. Higher load of 30 N resulted in an increased rate of wear. Furrows and delaminated areas were present in Fig. 13 and exhibited the adhesive and abrasive wear mechanism. At a load of 20 N, the top surfaces were identified with some oxide particles which may be due to higher temperature and friction heat generated during sliding. Due to continuous sliding condition, some oxide debris filled the gap on the pin outward and acted as a protective layer and the wear rate is mild. The oxide debris were present on the worn surface and it is confirmed through the elemental analysis (Fig. 7).

The metal removal rate was low at 20 N with all level of temperature which showed the oxidation wear mechanism [41]. Increase in load from 20 to 25 N resulted in the occurrence of delamination wear. The delamination concept maintains that plastic distortion, crack initiation and propagation leads to layer by layer delamination. The penetration of hard counter surface on the softer pin surface might have led to the displacement and rupture of the material. At high temperature level, removal of material increased with applied load. The deformed metallic layers moved according to the sliding direction. It resulted in slight increase of wear rate due to exclusion of wear debris. No oxide layer was present over the pin surface tested under higher load. The worn out surfaces exhibited the presence of flakes and grooves depicting severe abrasive wear.

5. Conclusion

The RSM based Box-Behnken design technique was successfully used to create the model for laser surface alloying of Cr_3C_2-25% NiCr on NCI. The suitability of the developed model for tribological studies was confirmed using ANOVA. Based on the experimental results and modeling by RSM, the following conclusions were drawn.

The surface alloyed at 1.5 kW laser power and 600 mm/min scan speed with 15 mm defocus and 30% overlapping resulted as the optimized laser process parameter. As the cooling rate plays a vital role in laser surface alloying process, the decrease in laser power and speed reduced the cooling rate and resulted surface cracks in LSA region.

- The presence of elongated eutectic carbide in the Cr_3C_2-25% NiCr laser alloyed specimen greatly improved the wear resistance property of the substrate material. The fine cellular dendrite structure produced during laser treatment also improved the microhardness of the base material by more than 4 times
- The ANOVA results indicated that the predicted R^2 value (0.94939) is also in good agreement with Adj. R^2 value (0.99083) and the reliability of the developed model is most significant for determining the wear rate.
- The developed material removal mechanism plots indicates that the value of CoF decrease with the increase in applied load and sliding velocity. The wear rate increases with the increase of applied load and sliding velocity.
- The perturbation plot indicated that the applied load leads to increase in wear at the contact area. When it comes to

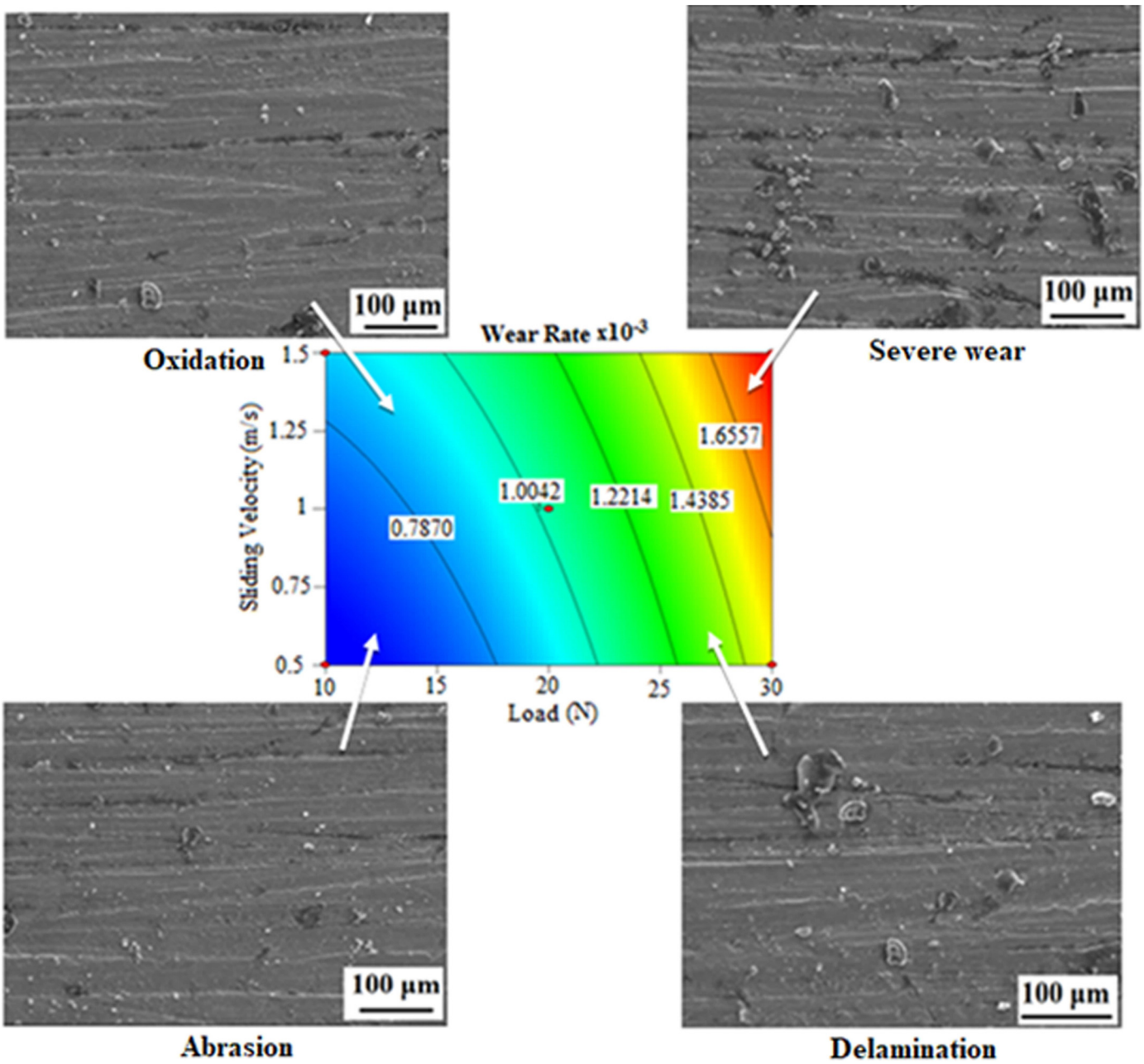

Fig. 13. Wear mechanism of laser alloyed sample

sliding velocity and temperature, the effect on wear rate is very less, as the coated materials enhanced the tribological properties on the base material.

REFERENCES

[1] H. Yan, A. Wang, Z. Xiong, K. Xu, Z. Huang, Applied Surface Science. **256** (23), 7001-009 (2010).

[2] K.Y. Benyounis, O.M.A. Fakron, J.H. Abboud, A.G. Olabi, M.J.S. Hashmi, J. Mater. Process. Technol. **170** (1-2), 127-132 (2005).

[3] E. Jonda, Z. Brytan, K. Labisz, A. Drygała, Arch. Metall. Mater. **61** (3), 1309-1314 (2016). DOI: 10.1515/amm-2016-0216.

[4] M. Bonek, Arch. Metall. Mater. **59** (4), 1647-1651 (2014). DOI: 10.2478/amm-2014-0280.

[5] A.R. da Costa, A. Craievich, R. Vilar, Mater. Sci. Eng. A. **336** (1-2), 215-218 (2002).

[6] Q.B. Liu, H. Liu, J. Mater. Process. Technol. **88**, 77-82 (1999).

[7] W. Tarasiuk, A.I. Gordienko, A.T. Wolocko, J. Piwnik, B. Szczucka-Lasota, Arch. Metall. Mater. **60** (4), 2939-2943 (2015). DOI: 10.1515/amm-2015-0469.

[8] W.P. Jiang, P. Mollan, Surf. Coat. Technol. **135**, (2-3), 139-149 (2001).

[9] B.S. Yilbas, S.Z. Shuja, S.M.A. Khan, A. Aleem, Appl. Surf. Sci. **255** (23), 9396-9403 (2009).

[10] W.L. Xu, T.M. Yue, H.C. Man, C.P. Chan, Surf. Coat. Technol. **200** (16-17), 5077-5086 (2006).

[11] J.H. Yao, L. Wang, Q. Zhang, F.Z. Kong, C.H. Lou, Z.J. Chen, Opt. Laser Technol. **40**, 838-843 (2008).

[12] M.L. Zhong, W.J. Liu, H.J. Zhang, Wear. **260**, 1349-1355 (2006).

[13] B.G. Guo, J.S. Zhou, S.T. Zhang, H.H. Zhou, Y.P. Pu, J.M. Chen, Mater. Sci. Eng. A. **480**, 404-410 (2008).
[14] A.H. Wang, X.L. Zhang, X.F. Zhang, X.Y. Qiao, H.G. Xu, C.S. Xie, Mater. Sci. Eng. A. **475**, (1-2), 312-318 (2008).
[15] M. Bonek, Arch. Metall. Mater. **61** (2), 719-724 (2016). DOI: 10.1515/amm-2016-0123.
[16] J. He, J.M. Schoenung, Mater. Sci. Eng. A. **336**, 274-319 (2002).
[17] Sivarao, Shukor, T.J.S. Anand, Ammar, Int. J. of Eng. Techn. **10** (4), 1-7 (2010).
[18] F.H. Stott, D.S. Lin, G.F. Wood, C.W. Stevenson, Wear. **36** (2), 147-74 (1969).
[19] R. Kumar, S. Dhiman, Materials Design. **50**, 351-359 (2013).
[20] J.F. Lin, C.C. Chou, Tribology International. **35** (11), 771-785 (2002).
[21] M.C.M. Farias, R.M. Souza, A. Sinatora, D.K. Tanaka, Wear. **263** (1-6), 773-781 (2007).
[22] Y. Sahin, K.A. Ozdin, Materials and Design. **29** (3), 728-733 (2008).
[23] Standard test method for wear testing with a pin-on-disk apparatus, ASTM Standard. G: 99-05 (2010).
[24] S. Rajakumar, C. Muralidharan, V. Balasubramanian, Trans. Non Ferr. Mat. Soc. **20** (10), 1863-72 (2010).
[25] S.C. Vettivel, N. Selvakumar, R. Narayanasamy, N. Leema, Materials and Design. **50**, 977-996 (2013).
[26] S. Rajakumar, C. Muralidharan, V. Balasubramanian, Mater Des. **32** (5), 2878-90 (2011).
[27] R. Narayanasamy, M. Ravichandran, C. Sathiya Narayanan, N.L. Parthasarathi, R. Ravindran, Int. J. Mech. Mater. Des. **3** (4), 293-307 (2006).
[28] D. Prabhakaran, CA. Basha, T. Kannadasan, P. Aravinthan, J. Environ Sci. Health Part A. **45** (4), 400-12 (2010).
[29] A. K. Lakshminarayanan, V. Balasubramanian, Trans Non Ferr Met Soc. **19** (1), 9-18 (2009).
[30] W. Xiao, S. Xinhua, J. Minfeng, L. Pin, H. Yang, W. Kai, Opt. Las. Technol. **44** (3), 656-63 (2012).
[31] P. Dinesh Babu, G. Buvanashekaran, K.R. Balasubramanian, Tribology Transactions. **58** (4), 602-615 (2015).
[32] A. Gulzar, J.I. Akhter, M. Ahmad, G. Ali, M. Mahmood, M. Ajmal, Appl. Surf. Sci. **255** (20), 8527-8532 (2009).
[33] Y. Chen, C.H. Gan, L.X. Wang, G. Yu, A. Kaplan, Appl. Surf. Sci. **245** (1-4), 316-321 (2005).
[34] D.W. Zeng, C.S. Xie, K.C. Yung, Mater. Sci. Eng. A. **333**, 223-231 (2002).
[35] N. Jeyaprakash, M. Duraiselvam, S.V. Aditya, Surface Review. and Letters. **26**, 1950009 (2019).
[36] L. Pengting, L. Yunguo, W. Yuying, M. Guiong, L. Xiangfa, Mater. Sc. Eng. A. **546**, 146-52 (2012).
[37] B. Bhushan, W.E. Jahsman, Int. J. Solids and Struc. **14** (1), 39-51 (1978).
[38] B. Bhushan, W.E. Jahsman, Int. J. Solids and Struc. **14** (9), 739-753 (1978).
[39] M.A. Chowdhury, M.M. Helali, Tribology International. **41** (4), 307-314 (2008).
[40] K. Velmanirajan, A.S. Abu Thaheer, R. Narayanasamy, C.A. Basha, Mater. Des. **41**, 239-54 (2012).
[41] S. Anbuselvan, S. Ramanathan, Mater. Des. **31** (4), 1930-6 (2010).